



Nitro–Nitrito Photoisomerization of Cationic Platinum(II) Complexes in the Solid State: Reactivity in Polymorphic Crystals and Glassy State

Nakamura, Ibuki

Sumitani, Ryo

Mochida, Tomoyuki

(Citation)

Crystal Growth & Design, 21(3):1861–1868

(Issue Date)

2021-03-03

(Resource Type)

journal article

(Version)

Accepted Manuscript

(Rights)

This document is the Accepted Manuscript version of a Published Work that appeared in final form in Crystal Growth & Design, copyright © American Chemical Society after peer review and technical editing by the publisher. To access the final edited and published work see <https://doi.org/10.1021/acs.cgd.1c00004>

(URL)

<https://hdl.handle.net/20.500.14094/90008230>



Nitro-Nitrito Photoisomerization of Cationic Platinum(II) Complexes in the Solid State: Reactivity in Polymorphic Crystals and Glassy State

Ibuki Nakamura,^a Ryo Sumitani,^a and Tomoyuki Mochida^{ab}*

^aDepartment of Chemistry, Graduate School of Science, Kobe University, Rokkodai, Nada, Kobe, Hyogo 657-8501, Japan. E-mail: tmochida@platinum.kobe-u.ac.jp

^bCenter for Membrane Technology, Kobe University, Rokkodai, Nada, Kobe, Hyogo 657-8501, Japan

ABSTRACT: Nitro–nitrito isomerization is a well-known photoreaction exhibited by metal complexes in the solid state. We previously reported that the isomerization ratio in the salts of a cationic platinum(II) nitrito complex $[\text{Pt}(\text{L})(\text{NO}_2)]^+$ ($\text{L} = N^1$ -(2-(dimethylamino)ethyl)- N^2,N^2 -dimethyl- N^1 -pentyl-1,2-ethanediamine) is correlated to the reaction cavity surrounding the nitrito ligand. In this study, to further elucidate the effect of the packing structure on the reaction, we investigated the photoisomerization of the same cation in different packing environments. The salt of the cationic complex with the PF_6 anion gave three polymorphs (α -, β -, and γ -forms) and a pseudopolymorph (δ -form, acetonitrile solvate), of which the γ -form is formed from the δ -form upon desorption of acetonitrile. These polymorphs exhibited 36–100% conversions at 180 K depending on the reaction cavity. In addition, the β -form exhibited a space group change upon photoirradiation. The salt with the $(\text{CF}_3\text{SO}_2)_2\text{N}^-$ anion was an ionic liquid, taking both the crystalline and glassy states at low temperature. The crystalline state exhibited approximately 30% conversion at 100 K, whereas photoisomerization was not observed in its glassy state as investigated by IR spectroscopy. In these salts, less densely packed crystals deteriorated upon photoirradiation.

INTRODUCTION

Photochemical reactions of molecular compounds in the solid state have attracted considerable attention for several years.¹⁻⁵ Nitro–nitrito photoisomerization is one of the most well-known solid-state photoreactions of metal complexes with nitrito ligands.^{6,7} In this linkage isomerization reaction, the thermodynamically stable nitro isomer (nitrito- κN) isomerizes to the nitrito isomer (nitrito- κO) upon ultraviolet (UV) photoirradiation (Figure 1). The *endo* isomer is usually observed, whereas the *exo* isomer is observed at an intermediate stage. Such photo-switching phenomena are important in terms of application to energy conversion, optical memory, electronic devices, etc., and the photoisomerization mechanism is under active investigation. Recently, Hatcher and Raithby investigated the nitro–nitrito photoisomerization of a number of metal complexes in detail using *in situ* photocrystallography, revealing varying degrees of conversion,^{5,8-11} with only a few complexes exhibiting 100% conversion.¹⁰⁻¹² Furthermore, Boldyreva and Naumov revealed that the photoisomerization of cobalt complexes leads to photomechanical properties.¹³⁻¹⁵ Studies on the photoisomerization of several ammine^{9,16-19} and organometallic²⁰ complexes have suggested that the conversion is related to the reaction cavity surrounding the NO₂ ligands. However, despite the long history of its investigation, the factors governing the photoreaction have not been well understood.

In our previous study, we quantitatively demonstrated that the nitro-nitrito conversion in crystals was governed by the reaction cavity surrounding the nitrito ligand.²¹ We investigated the photoisomerization of salts of a cationic chelate Pt^{II} complex [Pt(L)(NO₂)]⁺ (L = *N*¹-(2-(dimethylamino)ethyl)-*N*²,*N*²-dimethyl-*N*¹-pentyl-1,2-ethanediamine) with Pt(NO₂)₄²⁻ and FSA anions (**1-Pt(NO₂)₄** and **1-FSA**, Figure 2) by *in situ* photocrystallography and found a correlation between the conversion and reaction cavity volume. Correlation between the reactivity and reaction cavity has also been found for various reactions in molecular crystals.²²⁻²⁵

In this study, to further elucidate the effect of the packing structure on the reaction, we synthesized

salts of the Pt^{II} complex with PF_6 and $(\text{CF}_3\text{SO}_2)_2\text{N}$ anions (**1-PF₆** and **1-Tf₂N**, Figure 2). **1-PF₆** formed three polymorphs and a pseudopolymorph, whereas **1-Tf₂N** was an ionic liquid exhibiting both crystalline and glassy states at low temperature. These features enabled investigation of the photoisomerization of the same complex in different packing environments. Tf₂N is a bulky low-symmetry anion often used as a component of ionic liquids,²⁶ which we have used to synthesize a number of metal-containing ionic liquids.²⁷⁻³⁰ In addition, less densely packed crystals were found to exhibit crystal deterioration upon photoirradiation. Comparison of these and previously reported salts elucidated the effect of the crystal environment on the photoisomerization reaction.

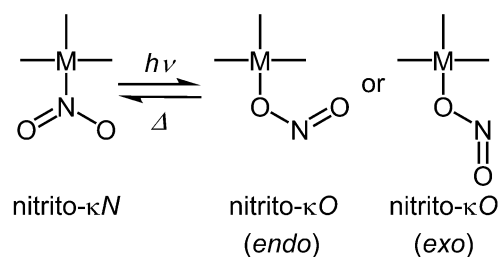


Figure 1. Nitro–nitrito linkage isomerization of metal complexes with a nitrito auxiliary ligand.

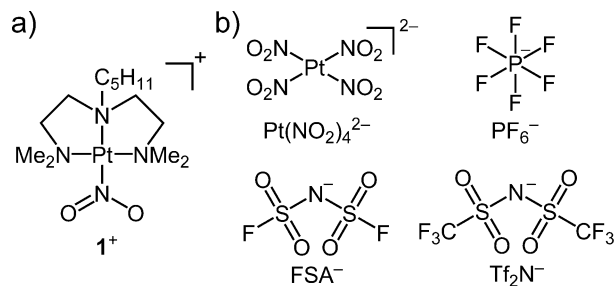


Figure 2. Structures of the (a) cation and (b) anions used in our study. The $\text{Pt}(\text{NO}_2)_4^{2-}$ and FSA^- anions were used in the previous study.²¹

RESULTS AND DISCUSSION

Synthesis and Thermal Properties. The obtained solid forms of **1-PF₆** and **1-Tf₂N** are summarized in Figure 3. **1-PF₆** gave three polymorphs, which are designated here as α -, β -, and γ -forms, of which

the α -form was dominantly obtained. The γ -form was obtained from a pseudopolymorph of an acetonitrile solvate (δ -form) by the loss of solvent in a few days when left in air. **1-Tf₂N** was obtained as a colorless ionic liquid, which formed a glassy state at a low temperature, but single crystals were also obtained by recrystallization from ethanol–diethyl ether. The thermal properties of α -**1-PF₆** and **1-Tf₂N** were investigated by differential scanning calorimetry (DSC) and thermogravimetry-differential thermal analysis (TG-DTA). The thermodynamic data are summarized in Table 1 along with those of **1-Pt(NO₂)₄** and **1-FSA** reported previously.²¹

The melting points of the crystals of α -**1-PF₆** and **1-Tf₂N** were 462.5 and 363.5 K, respectively. No phase transitions were observed down to 150 K in either salt. Upon cooling from the melt, α -**1-PF₆** exhibited crystallization, but **1-Tf₂N** exhibited a glass transition at 272 K. The DSC trace of **1-Tf₂N** is shown in Figure 4. The ratio of the glass transition temperature to the melting point (T_g/T_m) of **1-Tf₂N** was 0.75, which is comparable to the typical values for molecular liquids ($T_g/T_m = 2/3$).³¹ Pd^{II}-containing ionic liquids with the Tf₂N anion exhibiting similar thermal behavior have been reported previously.³²

The TG-DTA traces of these salts are shown in Figure 5. The decomposition temperatures of α -**1-PF₆** and **1-Tf₂N** (T_{dec} , 3 wt% weight loss temperature) were 519 and 517 K, respectively, which were similar to that of **1-FSA** ($T_{\text{dec}} = 523$ K). In the DTA trace of each salt, a large exothermic peak was observed around the decomposition temperatures, which is ascribed to the decomposition of the NO₂ ligand. α -**1-PF₆** exhibited a two-step weight loss similar to **1-FSA**,²¹ the first (~10 wt%, 510–530 K) and the second step (~40 wt%, 530–560 K) correspond to the losses of NO₂ (calculated value: 8 wt%) and chelate ligand (37 wt%), respectively. In contrast, **1-Tf₂N** exhibited a gradual weight loss.

Different solid forms of **1-PF₆** and **1-Tf₂N**

1-PF₆	α-form (82%)
	β-form (36%, 100%)
	γ-form (40%, deterioration)
	δ-form [MeCN solvate]
1-Tf₂N	Crystal state (28%, deterioration)
	Glassy state (0%)

Figure 3. Summary of the solid forms of the salts investigated in this study, with their photoisomerization ratios shown in parentheses.

Table 1. Melting Points (T_m), Melting Enthalpies (ΔH_m), Glass Transition Temperatures (T_g), and Decomposition Temperatures (T_{dec}) of the Synthesized Salts

complex	T_m/K	$\Delta H_m/kJ \cdot mol^{-1}$	T_g/K	T_g/T_m	T_{dec}^a/K
α - 1-PF₆	462.5	27.0	—	—	519
1-Tf₂N	363.5	20.5	272	0.75	517
1-FSA ^b	392.6	29.6	280	0.71	523
1-Pt(NO₂)₄ ^b	459.5	68.1	333	0.72	496

^aDetermined by TG analysis (3 wt% weight loss temperature).

^bRef. 21.

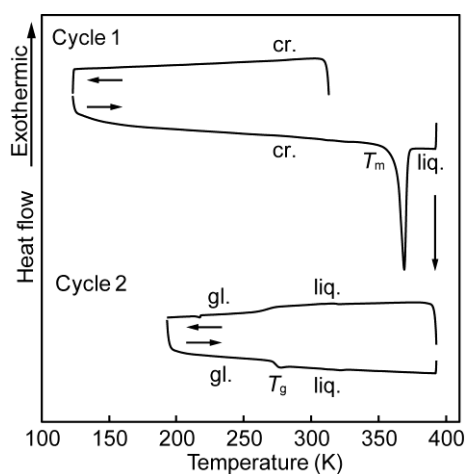


Figure 4. DSC traces of **1-Tf₂N** measured at 10 K min⁻¹, where cr., liq., and gl. stand for the crystal, liquid, and glassy states, respectively.

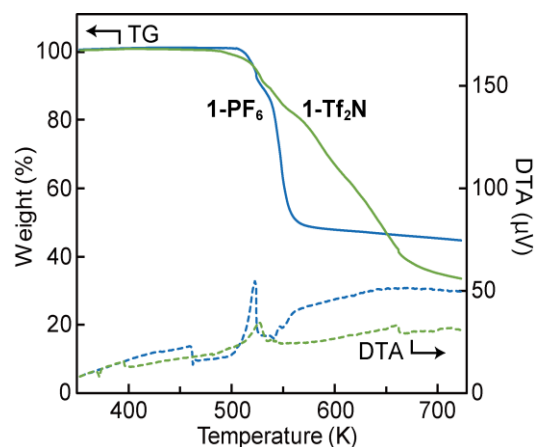


Figure 5. TG–DTA traces of α -**1-PF₆** (blue line) and **1-Tf₂N** (green line) measured under a nitrogen atmosphere at 3 K min⁻¹. The TG and DTA curves are represented by solid and dashed lines, respectively.

Crystal Structures of the 1-PF₆ Polymorphs. The crystal structures of the three polymorphs of **1-PF₆** (α -, β -, and γ -forms) were determined at 180 K. The structures determined at 100 K were almost identical to those at 180 K. The pseudopolymorph (δ -form) containing acetonitrile was also structurally characterized, which was isomorphous to the γ -form.

The packing diagrams of the α -, β -, and γ - forms are shown in Figure 6a–c. Their space groups were $P2_1$, $Pccn$, and $P2_1/c$, respectively. The cation structures in these crystals were almost the same, comprising a planar four-coordinate structure with a nitrito- κN coordination. The pentyl substituent in each cation adopted the all-*trans* conformation without disorder, except for the γ -form, as shown below. The anions were located near the coordination plane of the cation in each salt. The asymmetric units in the α - and γ - forms contain two crystallographically independent pairs of cations and anions (Figure 6a and c), whereas, that in the β -form, contains only one. Their packing efficiencies varied, as discussed later.

The packing structure of the δ -form (acetonitrile solvate) is shown in Figure 6d. The crystal was

isomorphous to the γ -form (Figure 6c); hence, the packing structure was maintained after the loss of the solvate molecule. The occupancy of the solvate molecule was 0.5, and the molecules were accommodated in a one-dimensional channel running along the a -axis, which accounts for its easy loss. The unit cell volumes at 180 K before and after the solvent loss were 4540.8(8) Å³ and 4503.9(4) Å³, respectively, reduced by only 0.8%. Therefore, the crystal contains large voids after solvent loss. The molecular structures of the cation before and after solvent loss were almost identical. The alkyl chain in cation A exhibited an *all-trans* conformation, whereas, that in cation B, surrounding the solvate molecule channel and thereby thermally mobile, exhibited a partial *cis* conformation with larger thermal ellipsoids.

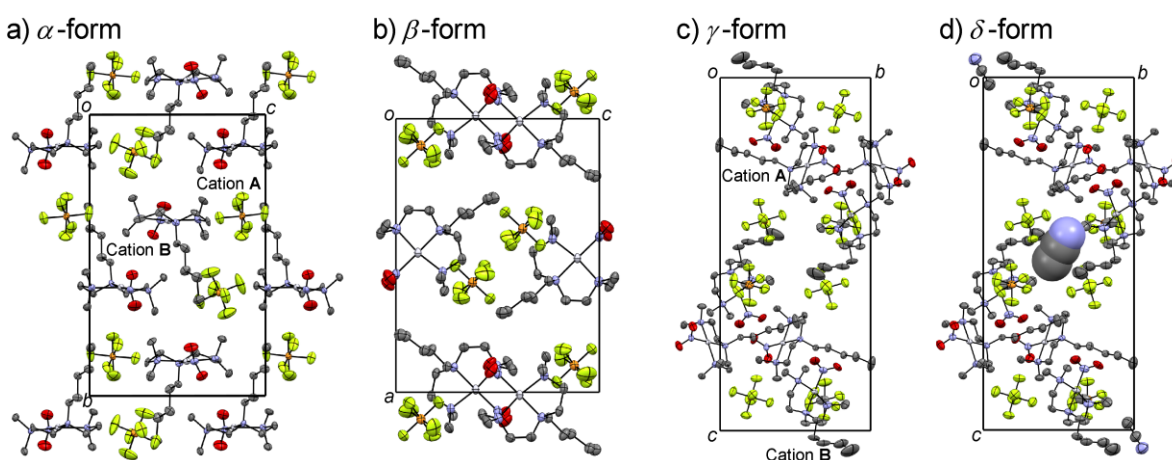


Figure 6. Packing diagrams of (a) α -, (b) β -, (c) γ -, and (d) δ -forms of **1-PF₆** at 180 K. The solvate molecule in (d) is displayed in the CPK model. The hydrogen atoms have been omitted for clarity.

Photoisomerization of the 1-PF₆ Polymorphs. The polymorphs of the PF₆ salts exhibited different photoisomerization behaviors, as examined by X-ray crystallography. The photoirradiation was conducted at 180 K to suppress thermal relaxation. After photoirradiation for 13 h, the α -form exhibited 82% conversion, whereas the β -form exhibited a space group change, giving two crystallographically independent cations with 36% and 100% conversion. The γ -form exhibited 40%

conversion, followed by crystal deterioration.

The unit cell of the α -form contains two crystallographically independent cations (cations A and B, Figure 6a). The structures of cation A before and after photoirradiation (365 nm) for 13 h at 180 K are shown in Figure 7a. Cation B exhibited almost the same structural change (Figure S1 in the Supporting Information). After photoirradiation, the nitrito ligands exhibited disorder and the population of the *endo*-nitrito- κO isomer increased. The conversion of cations A and B after 13 h of photoirradiation was 81% and 83%, respectively, which are within experimental error. The time course of the photoisomerization was almost the same as that of **1-FSA** and **1-Pt(NO₂)₄**,²¹ reaching almost constant after 4 h. After photoirradiation, anion B exhibited a two-fold rotational disorder (0.72:0.28), whereas anion A remained ordered. This cation–anion distance is longer for anion B (Pt–P_{PF₆(B)} = 6.0 Å) than for anion A (Pt–P_{PF₆(A)} = 4.9 Å), which may cause less efficient electrostatic interactions, allowing disorder. Slight expansion of the unit cell was observed after photoirradiation (+1.3%), which is ascribed to the larger size of the nitrito- κO isomer.^{9,10} To examine the thermal relaxation effect, after 13 h data collection, the sample was left in darkness at 180 K for 4 h, and the structure determination was then performed again. The isomer population decreased by only a few percent, similar to **1-Pt(NO₂)₄**,²¹ indicating that the thermal reverse reaction was not significant at this temperature. Photoisomerization was not crystallographically observed after photoirradiation at 293 K, owing to thermal relaxation.

The photoisomerization of the α -form was also detected using IR spectroscopy. After photoirradiation for 1 h at 180 K, peaks appeared at 1080 and 1425 cm^{−1}, associated with the decreasing intensity of the peak at 1370 cm^{−1} (Figure S2 in the Supporting Information). The spectrum before photoirradiation was recovered when the sample was heated to 300 K owing to thermal relaxation. The nitrito- κO and nitrito- κN stretching frequencies estimated by density functional theory (DFT) calculations were 1043 and 1368 cm^{−1}, respectively, consistent with the spectral changes, which are similar to those of **1-Pt(NO₂)₄**, **1-FSA**²¹ and related compounds.³³

Photoisomerization of the β -form accompanied a space group change from orthorhombic $Pccn$ to monoclinic $P2_1/c$, although the unit cells were almost identical. This structural transformation is unprecedented, but there are examples of space group changes upon nitro-nitrito and other photoisomerization reactions.^{34,35} In the current case, the packing structure was essentially unchanged upon photoirradiation, but the number of crystallographically independent cations doubled (Figure 7b). The resulting two cations with different environments exhibited different conversions after 13 h of photoirradiation: 36% for cation A (only the *exo*-nitrito- κO isomer) and 100% for cation B (a mixture of 42% *exo* and 58% *endo* nitrito- κO isomers). The unit cell volume increased by only 0.6%.

Photoirradiation of the γ -form for several hours resulted in the deterioration of the crystal, although structural analysis after 1 h of photoirradiation at 180 K was possible. The pentyl substituents in the cations and anions exhibited disordered structures, and the conversion was 39% and 40% for molecules A and B, respectively, which are within experimental error (Figure S3 in the Supporting Information). No further discussion is given owing to the low data quality. Structure determination after photoirradiation at 100 K failed. The deterioration of the crystals is ascribed to the porosity of the crystal, as discussed later.

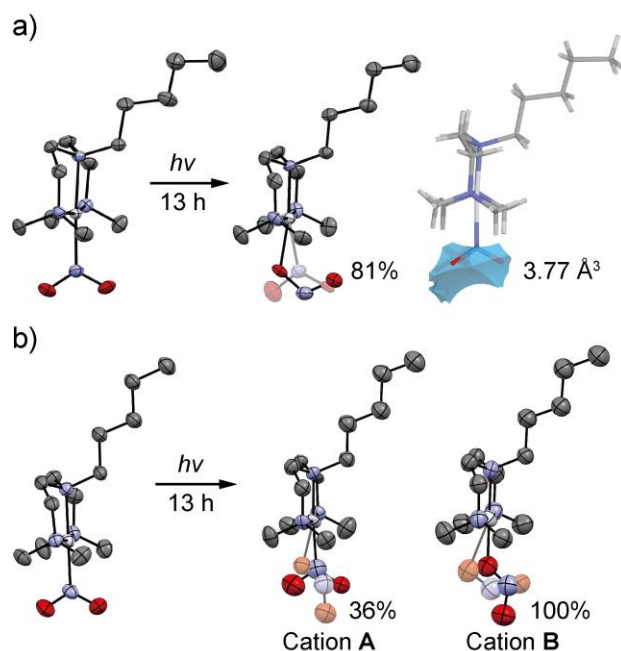


Figure 7. Molecular structures of the cations in (a) α -**1-PF₆** (cation A) and (b) β -**1-PF₆** at 180 K before and after photoirradiation for 13 h. The lower occupancy moieties in the disordered parts are shown in gray. Reaction cavity surrounding the NO₂ ligand is also shown in (a). The hydrogen atoms have been omitted for clarity.

Correlation between Reaction Cavity Volume and Conversion. As reported in our previous study,²¹ the nitro-nitrito photoisomerization reaction is governed by the reaction cavity surrounding the NO₂ ligand. The reaction cavity also accounts for the observed difference in the photoreactions of the polymorphs of **1-PF₆**.

The reaction cavity surrounding the nitrito ligand in each salt was calculated for the 180 K structure before photoirradiation. The reaction cavity is defined as the space surrounded by the spheres of atoms surrounding the ligand, and the radius of the sphere is larger by 1.2 Å than the van der Waals radii of the corresponding atom.²³ The reaction cavity volumes are listed in Table 2 along with the conversion in each salt. The reaction cavities of cations A and B in the α -form are shown in Figure 7a and Figure S1 in the Supporting Information, respectively. They have relatively large reaction cavities of 3.77 and 3.44 Å³, respectively. The reaction cavities for the β - and γ -forms are shown in Figure 7b and Figure S4 in the Supporting Information, respectively. The β -form has a smaller reaction cavity (2.74 Å³) than the α -form, whereas the γ -form has the smallest cavity (1.50 Å³ for cation A and 1.48 Å³ for cation B). The reaction cavity volumes at 100 K were also calculated (Table 2), which are generally smaller than those at 180 K owing to thermal contraction.

The conversion after 13 h of photoirradiation in these salts is plotted in Figure 8 versus the reaction cavity volume at 180 K, including the data for **1-Pt(NO₂)₄** and **1-FSA**.²¹ The plot indicates that the conversion increases with an increase in reaction cavity volume, though the conversion may be also affected by the reaction cavity shape. The higher conversion of **1-FSA** than the overall trend might thus

be ascribed to its cavity shape. The 1 h photoirradiation data are plotted for the γ -form, which may be regarded as an approximate value because approximately 90% of the saturation value is reached in 1 h in other salts. The β -form crystal exhibits a space group change upon photoirradiation, doubling the number of crystallographically independent cations. Therefore, the average conversion (68%) of cations A (36%) and B (100%) is plotted for this form, which agrees with the overall trend. Because the unit cell volume was almost identical (+0.6%) after photoirradiation, the different conversions for the two cations are ascribed to their reaction cavities becoming smaller and larger, respectively, with respect to the original cavity. To examine the origin of the complete conversion of cation B, the reaction cavity for the exo isomer of this molecule after photoirradiation was calculated (Figure S3 in the Supporting Information). The obtained cavity does not sterically allow the nitro isomer, which accounts for the high conversion. This result demonstrates the importance of the cavity shape, but the effect could not be quantitatively taken into account for the current discussion. The conversions at 180 K were compared in this study, but these may vary at different temperatures.^{12,20}

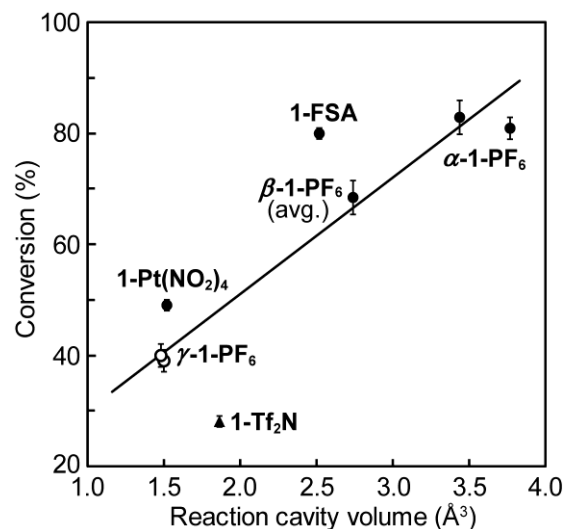


Figure 8. Conversion plotted as a function of reaction cavity volume. The data after photoirradiation for 13 h at 180 K (●), 1 h at 180 K (○), and 1 h at 100 K (▲) are plotted. The average conversion is

plotted for β -**1-PF₆**. The line represents the trend.

Table 2. Volume of Reaction Cavity Surrounding the Nitro Ligand (Å³) and Conversion (%) in Each Salt

complex	cavity volume/Å ³		conv. ^a /%
	100 K	180 K	
α - 1-PF₆ (cation A)	3.58	3.77	81(2)
(cation B)	3.46	3.44	83(3)
β - 1-PF₆ (cation A)	2.27	2.74	36(3)
(cation B ^b)	2.27	2.74	100(3)
γ - 1-PF₆ (cation A)	1.37	1.50	39(2) ^c
(cation B)	1.35	1.48	40(2) ^c
1-Tf₂N	1.87	2.42	28(1) ^{c,d}
1-FSA ^e	2.43	2.52	80(1)
1-[Pt(NO₂)₄] ^e	1.63	1.52	49(1)

^aAfter 13 h of photoirradiation at 180 K, unless otherwise noted. Estimated standard deviations are shown in parentheses. ^bCation B occurs after photoirradiation.

^cAfter 1 h of photoirradiation. ^dPhotoirradiation at 100 K.

^eRef. 21.

Crystal Structures of 1-Tf₂N. The crystal structure of **1-Tf₂N** was determined at 100 K and 180 K, and a disordered, less efficiently packed structure was observed at 180 K.

The packing diagram of **1-Tf₂N** is shown in Figure 9a. This salt crystallized in the space group *P2₁/c*, and the packing structure closely resembles that of **1-FSA**²¹ (Figure 9b) owing to the similar anion shapes. The molecular structures at 100 and 180 K are shown in Figures 10a and 10b, respectively. The thermal ellipsoids at 180 K were much larger than those at 100 K, and they were even larger than those of the cations in **1-PF₆** and other salts at the same temperature. Although there was no disorder at 100 K, both the cation and anion exhibited disorder at 180 K. The -CH₂CH₃ moiety in the cation exhibited a two-fold disorder (occupancy 0.82:0.18). One of the two CF₃ groups in the anion

exhibited a two-fold rotational disorder (0.5:0.5). The SO₂ moiety adjacent to the other CF₃ group in the anion also exhibited a two-fold disorder (0.79:0.21). Although the order–disorder of the Tf₂N anion often occurs through a phase transition,³⁶ no phase transition was detected by DSC measurements down to 120 K. The dihedral angle in the cation between the coordination plane and NO₂ ligand changed significantly with temperature, increasing from 44° at 100 K to 71° at 180 K. This is exceptional because the angles in the other salts were in the range of 72–83°, exhibiting almost no change with temperature (Table S1 in the Supporting Information).

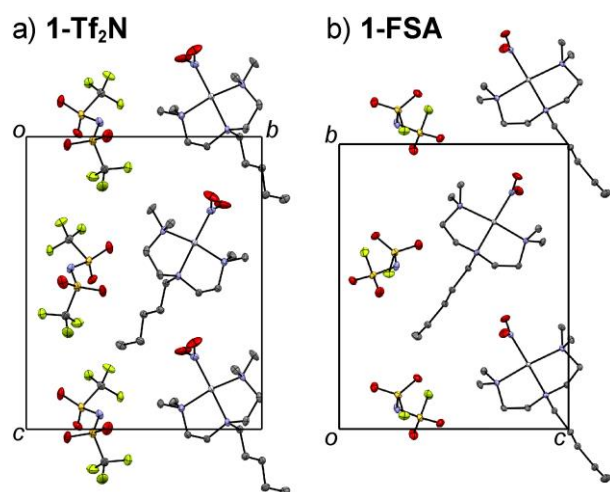


Figure 9. Packing diagrams of (a) **1-Tf₂N** and (b) **1-FSA**²¹ at 100 K. The hydrogen atoms have been omitted for clarity.

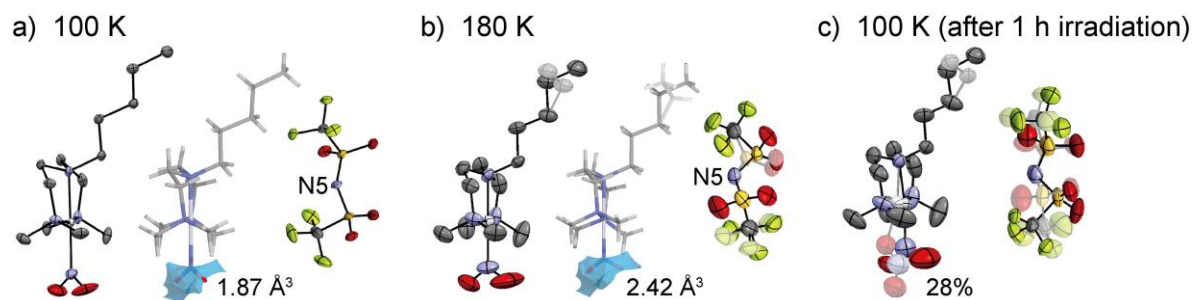


Figure 10. Molecular structures of the cation and anion in **1-Tf₂N** determined at (a) 100 K, (b) 180 K, and (c) after photoirradiation for 1 h at 100 K. The lower occupancy moieties in the disordered parts are

shown in gray. The reaction cavity surrounding the NO₂ ligand and its volume are also shown in (a) and (b). The hydrogen atoms have been omitted for clarity.

Photoisomerization of 1-Tf₂N. Photoirradiation of **1-Tf₂N** at 180 K resulted in severe deterioration of the crystal, whereas isomerization was observed at 100 K before deterioration.

Photoirradiation of the crystal at 180 K for 1 h caused a loss of crystallinity, observed as a gradual disappearance of diffraction spots. However, the structure could be determined after photoirradiation at 100 K for 1 h (Figure 10c), although longer photoirradiation again led to a loss of crystallinity. The NO₂ ligand exhibited 28% conversion to the *exo*-nitrito-κN isomer. In addition, both the cation and anion exhibited extensive disorder, though there was no disorder at 100 K before photoirradiation. The -CH₂CH₃ moiety and the metal center in the cation exhibited two-fold disorder (0.71:0.29 and 0.45:0.55, respectively), and the anion exhibited a severe two-fold rotational disorder.

The reaction cavities surrounding the NO₂ ligand of this salt are also shown in Figure 10a and b. The conversion in this salt (28%) is reasonable for the reaction volume of 1.9 Å³ at 100 K, as plotted in Figure 8, considering the short photoirradiation time. The reaction cavity in **1-Tf₂N** expanded from 1.87 Å³ at 100 K to 2.42 Å³ at 180 K (+29%, Table 2), which is exceptional because the temperature variation of the reaction cavity volume is much smaller in the other salts (1–21%).

The photoisomerization of **1-Tf₂N** in the glassy state formed upon cooling from the liquid state was investigated by IR spectroscopy. In contrast to the case of α-**1-PF₆**, no spectral change was observed upon photoirradiation for 1 h at 180 K, which indicates the absence of photoisomers. This is reasonable because the glassy state has high enthalpy and a less densely packed structure, allowing an efficient thermal relaxation. The IR spectrum of the **1-Tf₂N** crystal also exhibited no change after photoirradiation at 180 K, ascribed to the loss of crystallinity upon photoirradiation.

Comparison of Packing Efficiency. To compare the packing features of these salts qualitatively, their packing coefficients at 100 K and thermal expansion rates, defined here as the ratio of the unit cell volumes at 180 K vs 100 K, were calculated (Table 3). The data indicate that the observed photodeterioration tendency is correlated with the packing efficiency.

As seen in Table 3, γ -**1-PF₆** and **1-Tf₂N** have small packing coefficients (64.4% and 68.1%, respectively) compared with the other salts. The loss of crystallinity of these crystals upon photoirradiation at 180 K is probably due to the less densely packed, fragile structures, which are susceptible to local strain caused by photoisomerization. The small packing coefficient of γ -**1-PF₆** is ascribed to its porous structure formed by the loss of solvate molecules from the channel. This salt has an exceptionally small thermal expansion (0.8%) because the change in channel size compensates for the thermal expansion. The thermal expansion rate (2.9%) of **1-Tf₂N** was exceptionally large compared with those of the other salts (< 1.7%), which is ascribed to the development of disorder, as shown in the previous section. Therefore, the packing efficiency of this salt at 180 K is much lower than at 100 K, which is responsible for the crystal deterioration. The Tf₂N anion often exhibits disorder in the solid state with increasing temperature, causing less efficient packing.^{26,36} Therefore, the observed crystallographic features of **1-Tf₂N**, such as large thermal expansion of the reaction cavity, large thermal ellipsoids at 180 K, and a less efficient packing with disorder, are the consequences of using the Tf₂N anion. Notably, **1-Tf₂N** and **1-FSA** exhibited different photoreactivities despite their close structural resemblance, as seen in Figure 9.

1-Pt(NO₂)₄ is the only divalent salt in Table 3, having the largest packing coefficient (71.7%) and a much smaller thermal expansion rate (0.1%) than the other salts (1.5–2.9%). This tendency is consistent with the stronger cation–anion Coulomb interactions in the divalent salt. There was no correlation between the packing coefficient and reaction cavity size, indicating that the cavity size is governed by the local environment, not directly correlated with the overall packing efficiency.

Moreover, the unit cell volume, and therefore the packing efficiency, were almost unchanged after photoisomerization. The unit cell volumes of α -**1-PF₆** and **1-FSA**, which exhibited high conversion rates (~80%), increased by 1.3% and 1.8%,²¹ respectively, after 13 h of photoirradiation at 180 K.

Table 3. Packing Coefficients and Thermal Expansion Rates Calculated from Crystal Structures

complex	packing coefficient at 100 K (%)	thermal expansion ($V_{180K}/V_{100K}-1$, %)
α - 1-PF₆	69.4	1.5
β - 1-PF₆	67.9	2.0
γ - 1-PF₆	64.4	0.8
1-Tf₂N	68.1	2.9
1-FSA ^a	70.2	1.7
1-Pt(NO₂)₄ ^a	71.7	0.1

^aRef. 21.

CONCLUSIONS

Salts of a cationic platinum chelate complex bearing a nitrito auxiliary ligand were synthesized, and their nitro–nitrito photoisomerization behavior was investigated by *in situ* X-ray photocrystallography. The PF₆ salt gave several polymorphs, and their conversion varied at 36–100% depending on the reaction cavity surrounding the NO₂ ligand. In addition, the β -form exhibited a space group change upon photoirradiation. Their packing efficiency differed from each other, and the polymorph with a less efficiently packed structure exhibited crystal deterioration upon photoirradiation. The Tf₂N salt was an ionic liquid, taking both crystalline and glassy states at low temperature. The crystalline state exhibited isomerization, but deterioration occurred upon photoirradiation, ascribed to the tendency of the Tf₂N anion to form a disordered, less efficiently packed structure. Photoisomerization was not observed in the glassy state of the Tf₂N salt, which suggests efficient thermal relaxation of the photoexcited isomer

in the high enthalpy state. Thus, the photoisomerization of the same complex in different packing environments was investigated. In agreement with our previous results on the photoisomerization of salts with different anions, the reactivity of these salts correlated with the reaction cavity size, even though the reactivity was also affected by the cavity shape. Although the reaction cavity volume before photoirradiation was used in the current analysis, monitoring the change in the reaction cavity volume and shape during photoisomerization would provide a better understanding of the isomerization behavior in future analysis. Exploration of such photo-switching phenomena may also be important for potential applications.

EXPERIMENTAL SECTION

General Considerations. The ligand (L) 1,1,7,7-tetramethyl-4-pentyldiethylenetriamine was prepared according to the literature.²¹ ¹H NMR spectra were recorded using a Bruker Avance 400 instrument. Room-temperature FT-IR spectra were measured using a Thermo Scientific Nicolet iS5 FT-IR spectrometer attached to an ATR unit (diamond). Variable-temperature IR spectra were recorded for samples sandwiched between CaF₂ plates using a JASCO FT/IR-4700 spectrometer. Temperature control was performed using a UNISOKU cryostat CoolSpeK UV USP-203-A. DSC measurements were performed using a TA Q100 differential scanning calorimeter at a scan rate of 10 K min⁻¹. TG-DSC measurements were performed using a Rigaku TG8120 thermal analyzer at a scan rate of 3 K min⁻¹ under a nitrogen atmosphere. DFT calculations were performed using the Spartan '18 (Wavefunction Inc.) at the ωB97-D/LanL2DZ level (frequency scale factor: 0.942).

Synthesis of [Pt(L)(NO₂)]PF₆ (1-PF₆). An aqueous solution (0.7 mL) of K₂[Pt(NO₂)₄] (89 mg, 0.20 mmol) was added to an acetone solution (0.5 mL) of 1,1,7,7-tetramethyl-4-pentyldiethylenetriamine (41 mg, 0.18 mmol), and the solution was refluxed for 17 h. After evaporation of the solvent, the residue was dissolved in an aqueous solution (5 mL) of KPF₆ (130 mg, 0.70 mmol).

The solution was extracted with dichloromethane (5 mL \times 4), and the organic layer was dried over MgSO₄ before being evaporated. The resulting orange oil was dissolved in ethanol, and a white precipitate was formed. The precipitate was collected by filtration and dried under vacuum, the resulting powder was dissolved in a small amount of acetonitrile in a test tube, and diethyl ether was slowly layered onto the solution. Storing the solution at -4°C for 3 days gave colorless block crystals of the **α -1-PF₆** (25 mg, 38% yield). ¹H NMR (400 MHz, CD₃CN): δ = 3.44–3.25 (m, 4H, $H_{2,6,1}$), 3.05–2.92 (m, 10H, $H_{3,5,7}$), 2.81–2.72 (m, 6H, H_1), 1.55–1.47 (m, 2H, H_2), 1.42–1.28 (m, 2H, $H_{3,4}$), 0.95 (t, J = 0.71 Hz, 3H, H_5). FT-IR (ATR, cm⁻¹): 2960, 2868 (C-H), 1377, 1328 (NO₂), 556 (PF₆). Anal. Calcd. for C₁₃H₃₁F₆N₄O₂Pt: C, 25.37; H, 5.08; N, 9.10. Found: C, 25.84; H, 5.49; N, 9.17.

Synthesis of [Pt(L)(NO₂)]Tf₂N (1-Tf₂N). An aqueous solution (0.3 mL) of LiTf₂N (52 mg, 0.18 mmol) was added to an acetone solution (0.6 mL) of **1-PF₆** (62 mg, 0.10 mmol), and the mixture was stirred at room temperature for 2 h. After evaporation of acetone, the solution was extracted with dichloromethane (5 mL \times 6). The organic layer was washed with water (10 mL \times 2) and evaporated. The anion exchange procedure was repeated again, when the complete disappearance of the PF₆ anion was confirmed by ¹⁹F NMR spectra (CD₃CN). The resulting oil was dried under vacuum at 60°C for 14 h. The product was obtained as a colorless, highly viscous liquid (48 mg, 64% yield), and the liquid solidified upon repeated application of physical stimuli with a spatula. ¹H NMR (400 MHz, CD₃CN): δ = 3.44–3.25 (m, 4H, $H_{2,6,1}$), 3.05–2.92 (m, 10H, $H_{3,5,7}$), 2.80–2.72 (m, 6H, H_1), 1.55–1.47 (m, 2H, H_2), 1.42–1.28 (m, 2H, $H_{3,4}$), 0.95 (t, J = 0.71 Hz, 3H, H_5). ¹⁹F NMR (400 MHz, CD₃CN): δ = -80.24 (s, 6F, C-F). FT-IR (ATR, cm⁻¹): 2934, 2860 (C-H), 1385, 1333 (NO₂). Anal. Calcd. for C₁₅H₃₁F₆N₅O₆PtS₂: C, 24.00; H, 4.16; N, 9.33. Found: C, 24.31; H, 3.97; N, 9.19.

X-ray Crystallography. Single crystals of **α -1-PF₆** suitable for X-ray crystallography were obtained by diffusion of diethyl ether into an acetonitrile solution at -4°C . Single crystals of the β - and δ - forms were obtained under the same conditions on a few occasions. Each batch consisted of a single

form only. Leaving the δ -form under air resulted in the loss of the solvate molecule in a few days to give the γ -form. Single crystals of **1-Tf₂N** were obtained by the diffusion of diethyl ether into an ethanol solution.

The diffraction data were collected on a Bruker APEX II Ultra diffractometer using MoK α radiation at 100 K and 180 K. The structures were solved by direct methods using SHELXL,³⁷ and the crystallographic parameters are provided in Tables S2–S5 in the Supporting Information. The *in situ* photocrystallography was conducted at 180 K, using a Hamamatsu LC-L1 V3 lightningcure UV-LED (365 nm) as the light source. The effect of surface absorption is insignificant owing to the small absorption coefficient of the cation ($37 \text{ M}^{-1}\text{cm}^{-1}$)²¹ at 365 nm. The LED was positioned 3.3 cm from the sample (power density 55 mW/cm^2), and the crystal was rotated by 90° every 15 min during photoirradiation. The diffraction data were collected over 2 h, in darkness, following periods of 1, 4, and 13 h of photoirradiation. β -**1-PF₆** exhibited slight crystal deterioration upon photoirradiation due to structural transformation. The unit cell could not be determined after 1 h of photoirradiation owing to diffraction spot overlap, while the transformation was complete after 4 h of photoirradiation. The experiments for γ -**1-PF₆** and **1-Tf₂N** were also conducted at 100 K because crystal deterioration occurred after photoirradiation at 180 K, though the data quality obtained from γ -**1-PF₆** was still low due to crystal deterioration (one alert A and one alert B). Therefore, the γ -**1-PF₆** data are in the Supporting Information. The reaction cavities were calculated using the Cavity v5.0 program.²⁴ The packing indices were calculated using PLATON.³⁸

ASSOCIATED CONTENT

Supporting Information

The Supporting Information is available free of charge at <http://pubs.acs.org/doi/10.1021/acs.cgd>.

Molecular structures, IR spectra, bond lengths and angles, and crystallographic parameters (PDF).

Accession Codes

CCDC 1900144–1900145, 1922722–1922724, and 2052758–2052764 contain the supplementary crystallographic data for this paper. These data can be obtained free of charge via www.ccdc.cam.ac.uk/data_request/cif, or by emailing data_request@ccdc.cam.ac.uk, or by contacting The Cambridge Crystallographic Data Centre, 12 Union Road, Cambridge CB2 1EZ, UK; fax: +44 1223 336033.

AUTHOR INFORMATION

Corresponding Author

Tomoyuki Mochida - Department of Chemistry, Graduate School of Science and Center for Membrane Technology, Kobe University, Rokkodai, Nada, Kobe, Hyogo 657-8501, Japan; orcid.org/0000-0002-3446-2145; Phone: +81-78-803-5679.

E-mail: tmochida@platinum.kobe-u.ac.jp.

Authors

Ibuki Nakamura - *Department of Chemistry, Graduate School of Science, Kobe University, Rokkodai, Nada, Kobe, Hyogo 657-8501, Japan*

Ryo Sumitani - *Department of Chemistry, Graduate School of Science, Kobe University, Rokkodai, Nada, Kobe, Hyogo 657-8501, Japan; orcid.org/0000-0002-6617-2994*

Complete contact information is available at:

<http://pubs.acs.org/doi/10.1021/acs--->.

Notes

The authors declare no competing financial interest.

ACKNOWLEDGMENTS

This work was financially supported by KAKENHI (grant numbers 20H02756) from the Japan Society for the Promotion of Science (JSPS).

REFERENCES

- (1) Vittal, J.J.; Quah, H. S. Photochemical reactions of metal complexes in the solid state. *Dalton Trans.* **2017**, 46, 7120–7140.
- (2) Simmons, E.L.; Wendlandt, W.W. Solid-state photochemical reactions of transition-metal coordination compounds. *Coord. Chem. Rev.* **1971**, 7, 11–27.
- (3) Coppens, P.; Novozhilova, I.; Kovalevsky, A. Photoinduced Linkage Isomers of Transition-Metal Nitrosyl Compounds and Related Complexes. *Chem. Rev.* **2002**, 102, 861–884.
- (4) Coppens, P.; Vorontsov, I. I.; Graber, T.; Gembicky, M.; Kovalevsky, A. Y. The structure of short-lived excited states of molecular complexes by time-resolved X-ray diffraction. *Acta Crystallogr. Sect. A* **2005**, 61, 162–172.
- (5) Hatcher, L. E.; Skelton, J. M.; Warren, M. R.; Raithby, P. R. Photocrystallographic Studies on Transition Metal Nitrito Metastable Linkage Isomers: Manipulating the Metastable State. *Acc. Chem. Res.* **2019**, 52, 1079–1088.
- (6) Grenthe, I.; Nordin, E. Nitrito-nitro linkage isomerization in the solid state. 2. A comparative study of the structures of nitrito- and nitropentaaminecobalt(III) dichloride. *Inorg. Chem.* **1979**, 18, 1869–1874.
- (7) Awasabisah, D.; Richter-Addo, G.B. Chapter One - NO_x Linkage Isomerization in Metal Complexes, In *Advances in Inorganic Chemistry*, Van Eldik, R. Olabe, J.A. (Eds.), Academic Press, **2015**, 67, 1–78.
- (8) Warren, M. R.; Brayshaw, S. K.; Hatcher, L. E.; Johnson, A. L.; Schiffers, S.; Warren, A. J.; Teat, S. J.; Warren, J. E.; Woodall, C. H.; Raithby, P. R. Photoactivated linkage isomerism in single crystals of nickel, palladium and platinum di-nitro complexes – a photocrystallographic investigation.

Dalton Trans. **2012**, 41, 13173–13179.

- (9) Hatcher, L. E.; Skelton, J. M.; Warren, M. R.; Stubbs, C.; Lora da Silva, E.; Raithby, P. R. Monitoring photo-induced population dynamics in metastable linkage isomer crystals: a crystallographic kinetic study of [Pd(Bu₄dien)NO₂]BPh₄. *Phys. Chem. Chem. Phys.* **2018**, 20, 5874–5886.
- (10) Hatcher, L. E. Raising the (metastable) bar: 100% photo-switching in [Pd(Bu₄dien)(η¹-NO₂)]⁺ approaches ambient temperature. *CrystEngComm* **2016**, 18, 4180–4187.
- (11) Hatcher, L. E.; Raithby, P. R. The impact of hydrogen bonding on 100% photo-switching in solid-state nitro–nitrito linkage isomers. *CrystEngComm* **2017**, 19, 6297–6304.
- (12) Kutniewska, S. E.; Krówczyński, A.; Kamiński, R.; Jarzemska, K. N.; Pillet, S.; Wenger, E.; Schaniel, D. Photocrystallographic and spectroscopic studies of a model (N,N,O)-donor square-planar nickel(II) nitro complex: in search of high-conversion and stable photoswitchable materials. *IUCrJ* **2020**, 7, 1188–1198.
- (13) Naumov, P.; Chizhik, S.; Panda, M. K.; Nath, N. K.; Boldyreva, E. V. Mechanically Responsive Molecular Crystals. *Chem. Rev.* **2015**, 115, 12440–12490.
- (14) Chizhik, S.; Sidelnikov, A.; Zakharov, B. A.; Naumov, P.; Boldyreva, E. V. Quantification of photoinduced bending of dynamic molecular crystals: from macroscopic strain to kinetic constants and activation energies. *Chem. Sci.* **2018**, 9, 2319–2335.
- (15) Naumov, P.; Sahoo, S. C.; Zakharov, B. A.; Boldyreva, E. V. Dynamic Single Crystals: Kinematic Analysis of Photoinduced Crystal Jumping (The Photosalient Effect). *Angew. Chem., Int. Ed.* **2013**, 52, 9990–9995.
- (16) Sidelnikov, A. A.; Chizhik, S. A.; Zakharov, B. A.; Chupakhin, A. P.; Boldyreva, E. V. The effect of thermal expansion on photoisomerisation in the crystals of [Co(NH₃)₅NO₂]Cl(NO₃): different strain origins – different outcomes. *CrystEngComm* **2016**, 18, 7276–7283.
- (17) Boldyreva, E.V. Crystal-Structure Aspects of Solid-State Inner-Sphere Isomerization in Nitro(nitrito)pentaamminecobalt(III) Complexes. *Russ. J. Coord. Chem.* **2001**, 27, 297–323.
- (18) Ohba, S.; Tsuchimoto, M.; Kurachi, S. Investigation of solid-state photochemical nitro–nitrito linkage isomerization: crystal structures of trans-bis-(ethyl-enedi-amine)(iso-thio-cyanato)-nitritocobalt(III) salts: thio-cyanate, chloride monohydrate, and perchlorate–thio-cyanate-(0.75/0.25). *Acta Crystallogr., Sect. E*, **2018**, 74, 1526–1531.
- (19) Kubota, M.; Ohba, S. Nitro-nitrito linkage photoisomerization in crystals of pentaamminenitrocobalt(III) dichloride. *Acta Crystallogr. Sect. B*. **1992**, 48, 627–632.

- (20) Kutniewska, S. E.; Kamiński, R.; Buchowicz, W.; Jarzemska, K. N. Photo- and Thermoswitchable Half-Sandwich Nickel(II) Complex: $[\text{Ni}(\eta^5\text{-C}_5\text{H}_5)(\text{IMes})(\eta^1\text{-NO}_2)]$. *Inorg. Chem.* **2019**, *58*, 16712–16721.
- (21) Nakamura, I.; Funasako, Y.; T. Mochida, T. Nitro-Nitrito Photoisomerization of Platinum(II) Complexes with $\text{Pt}(\text{NO}_2)_4^{2-}$ and $(\text{FSO}_2)_2\text{N}^-$ anions: Correlation between Isomerization Rate and Reaction Cavity, *Cryst. Growth Des.* **2020**, *20*, 8047–8052.
- (22) Ohashi, Y. *Crystalline State Photoreactions: Direct Observation of Reaction Processes and Metastable Intermediates*; Springer: Tokyo, Japan, **2014**.
- (23) Ohashi, Y.; Yanagi, K.; Kurihara, T.; Sasada, Y.; Ohgo, Y. Crystalline state reaction of cobaloxime complexes by X-ray exposure. 1. A direct observation of Co–C bond cleavage in [(R)-1-cyanoethyl][(S)-(-)- α -methylbenzylamine]bis-(dimethylglyoximate)cobalt(III). *J. Am. Chem. Soc.* **1981**, *103*, 5805–5812.
- (24) Yamazaki, Y.; Sekine, A.; Uekusa, H. In Situ Control of Photochromic Behavior through Dual Photo-Isomerization Using Cobaloxime Complexes with Salicylidene-3-aminopyridine and 3-Cyanopropyl Ligands. *Cryst. Growth Des.* **2017**, *17*, 19–27.
- (25) Funasako, Y.; Ason, M.; Takebayashi, J.-i.; Inokuchi, M. Solid-State Photochromism of Salts of Cationic Spiropyran with Various Anions: A Correlation between Reaction Cavity Volumes and Reactivity. *Cryst. Growth Des.* **2019**, *19*, 7308–7314.
- (26) Kar, M.; Matuszek, K.; MacFarlane, D.R. Ionic liquids. *Kirk-Othmer Encyclopedia of Chemical Technology*, John Wiley & Sons, Inc., Hoboken, **2019**.
- (27) Tominaga, T.; Mochida, T. Multifunctional ionic liquids from rhodium(I) isocyanide complexes: Thermochromic, fluorescence, and chemochromic properties based on Rh-Rh interaction and oxidative addition. *Chem. Eur. J.* **2018**, *24*, 6239–6247.
- (28) Funasako, Y.; Mochida, T.; Takahashi, K.; Sakurai, T.; Ohta, H. Vapochromic Ionic Liquids from Metal-Chelate Complexes Exhibiting Reversible Changes in Color, Thermal and Magnetic Properties. *Chem. Eur. J.* **2012**, *18*, 11929–11936.
- (29) Funasako, Y.; Inagaki, T.; Mochida, T.; Sakurai, T.; Ohta, H.; Furukawa, K.; Nakamura, T. Organometallic ionic liquids from alkyloctamethylferrocenium cations: thermal properties, crystal structures, and magnetic properties. *Dalton Trans.* **2013**, *42*, 8317–8327.
- (30) Inagaki, T.; Mochida, T.; Takahashi, M.; Kanadani, C.; Saito, T.; Kuwahara, D. Ionic Liquids of Cationic Sandwich Complexes. *Chem. Eur. J.* **2012**, *18*, 6795–6804.
- (31) Turnbull, D.; Cohen, M. H. *Crystallization Kinetics and Glass Formation*. In *Modern Aspect of*

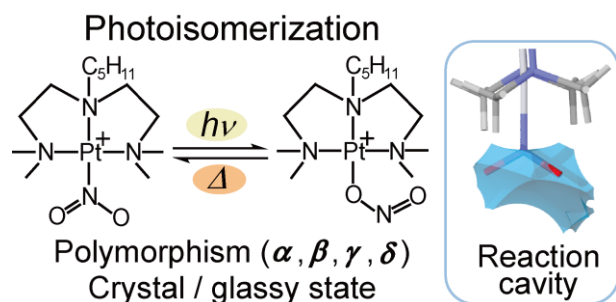
the Vitreous State, ed. MacKenzie, J. D. Butterworth & Co. Publishers Ltd., London, vol. 1, **1960**.

- (32) Hosokawa, H.; Funasako, Y.; Mochida, T. Ionic liquids from cationic palladium(II) chelate complexes: Preparation, thermal properties, and crystal structures. *Dalton Trans.* **2014**, *43*, 6864–6869.
- (33) Penland, R. B.; Lane, T. J.; Quagliano, J. V. Infrared Absorption Spectra of Inorganic Coordination Complexes. VII. Structural Isomerism of Nitro- and Nitritopentamminecobalt(III) Chlorides. *J. Am. Chem. Soc.* **1956**, *78*, 887–889.
- (34) Masciocchi, N.; Kolyshev, A.; Dulepov, V.; Boldyreva, E.; Sironi, A. Study of the Linkage Isomerization $[\text{Co}(\text{NH}_3)_5\text{NO}_2]\text{Br}_2 \rightleftharpoons [\text{Co}(\text{NH}_3)_5\text{ONO}]\text{Br}_2$ in the Solid State by x-ray Powder Diffraction. *Inorg. Chem.* **1994**, *33*, 2579–2585.
- (35) Taniguchi, T.; Sato, H.; Hagiwara, Y.; Asahi, T.; Koshima, H. Photo-triggered phase transition of a crystal. *Commun. Chem.* **2019**, *2*, 19.
- (36) Mochida, T.; Funasako, Y.; Inagaki, T.; Li, M.-J.; Asahara, K.; Kuwahara, D. Crystal Structures and Phase-Transition Dynamics of Cobaltocenium Salts with Bis(perfluoroalkylsulfonyl)amide Anions: Remarkable Odd–Even Effect of the Fluorocarbon Chains in the Anion. *Chem. Eur. J.* **2013**, *19*, 6257–6264.
- (37) Sheldrick, G. M. A short history of *SHELX*. *Acta Crystallogr., Sect. A: Found. Crystallogr.* **2008**, *64*, 112–122.
- (38) Spek, A. L. Structure validation in chemical crystallography. *Acta Crystallogr., Sect. D: Biol. Crystallogr.* **2009**, *65*, 148–155.

For Table of Contents Use Only

Nitro-Nitrito Photoisomerization of Cationic Platinum(II) Complexes in the Solid State: Reactivity in Polymorphic Crystals and Glassy State

Ibuki Nakamura, Ryo Sumitani, and Tomoyuki Mochida



The nitro–nitrito photoisomerization of a series of cationic Pt complexes has been investigated crystallographically. Polymorphic crystals exhibited varying conversions depending on the reaction cavity, and the glassy state exhibited no photoisomerization. Photoirradiation caused crystal deterioration in less efficiently packed crystals.

Supporting Information

Nitro-Nitrito Photoisomerization of Cationic Platinum(II) Complexes in the Solid State: Reactivity in Polymorphic Crystals and Glassy State

*Ibuki Nakamura,^a Ryo Sumitani,^a and Tomoyuki Mochida^{*a,b}*

^aDepartment of Chemistry, Graduate School of Science, Kobe University, Rokkodai, Nada, Kobe, Hyogo 657-8501, Japan. E-mail: tmochida@platinum.kobe-u.ac.jp

^bCenter for Membrane Technology, Kobe University, Rokkodai, Nada, Kobe, Hyogo 657-8501, Japan

Contents

Figure S1. Molecular structures of cation B in α -**1-PF₆**.

Figure S2. FT-IR spectra of α -**1-PF₆**.

Figure S3. Molecular structure of cation B in β -**1-PF₆**.

Figure S4. Molecular structures of the cations in γ -**1-PF₆**.

Table S1. Pt–N_{NO2} distances and dihedral angles between the Pt coordination plane and nitrito ligand.

Table S2–S5. Crystallographic parameters.

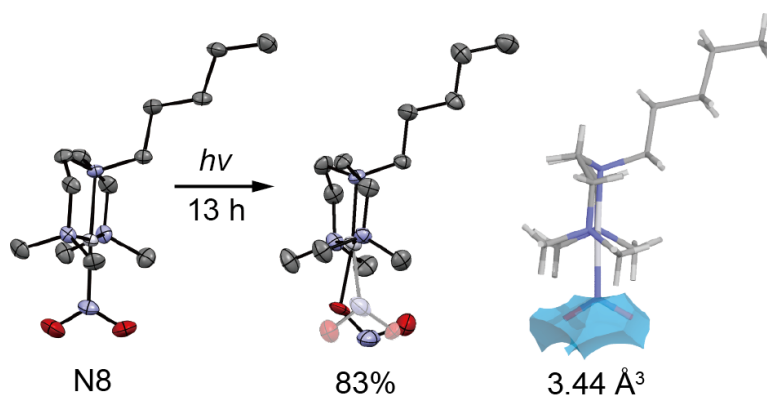


Figure S1. Molecular structures of cation B in α -1-PF₆ before and after photoirradiation for 13 h at 180 K. The lower occupancy moieties in the disordered parts are shown in gray. The reaction cavity surrounding the nitrito ligand is shown on the right.

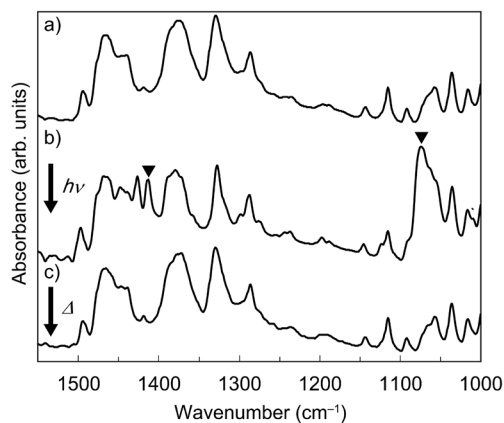


Figure S2. FT-IR spectra of α -1-PF₆ (a) before photoirradiation at 180 K, (b) after photoirradiation at 180 K for 1 h, and (c) after raising the temperature to 300 K. The nitrito- κ O stretching peaks are indicated by triangles in (b).

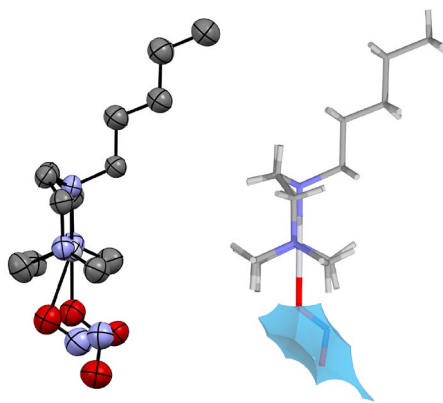


Figure S3. Molecular structure of cation B in β -1-PF₆ after photoirradiation for 13 h at 180 K. The reaction cavity surrounding the nitrito ligand is shown in the right figure.

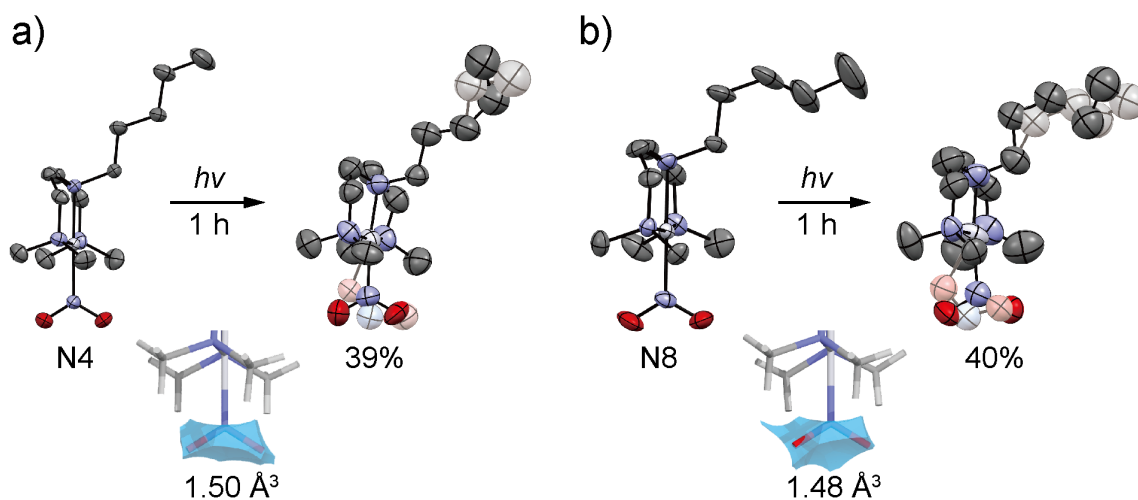


Figure S4. Molecular structures of (a) cation A and (b) cation B in γ -**1-PF₆** before and after photoirradiation for 1 h at 180 K. The reaction cavity surrounding the nitrito ligand are shown below.

Table S1. Pt–N_{NO₂} distances and dihedral angles between the Pt coordination plane and nitrito ligand.

Complex		Pt–N _{NO₂} distances (Å)		Dihedral angle (°)	
		100 K	180 K	100 K	180 K
α - 1-PF₆	Cation A	2.026(4)	2.024(5)	71.5	69.7
	Cation B	2.019(5)	2.015(5)	79.3	80.8
β - 1-PF₆		2.0219(18)	2.019(4)	82.1	85.7
γ - 1-PF₆	Cation A	2.012(2)	2.011(3)	71.2	70.8
	Cation B	2.007(2)	2.005(3)	63.5	67.8
δ - 1-PF₆	Cation A		2.022(5)		70.6
	Cation B		2.016(6)		69.2
1-Tf₂N		2.013(2)	1.987(5)	44.0	70.8

Table S2. Crystallographic parameters of α -1-PF₆

	α -1-PF ₆ _100K	α -1-PF ₆ _180K	α -1-PF ₆ _180K_13h
Empirical formula	C ₁₃ H ₃₁ F ₆ N ₄ O ₂ PPt		
Formula weight	615.48		
Crystal system	Monoclinic	Monoclinic	Monoclinic
Space group	$P2_1$	$P2_1$	$P2_1$
a [Å]	8.9363(6)	8.9852(12)	9.0850(11)
b [Å]	19.3540(12)	19.423(3)	19.525(2)
c [Å]	12.5405(8)	12.7082(18)	12.7139(15)
β [°]	106.2750(10)	106.836(2)	107.4700(10)
V [Å ³]	2082.0(2)	2122.8(5)	2151.2(4)
Z	4	4	4
ρ_{calcd} [g cm ⁻³]	1.964	1.926	1.900
$F(000)$	1200	1200	1200
Temperature [K]	100	180	180
Reflns collected	11660	11782	12157
Independent reflns	7983	7632	7750
Parameters	498	498	609
R (int)	0.0202	0.0207	0.0373
R_1^a, R_w^b ($I > 2\sigma$)	0.0182, 0.0409	0.0299, 0.0665	0.0358, 0.0927
R_1^a, R_w^b (all data)	0.0188, 0.0411	0.0313, 0.0670	0.0375, 0.0935
Goodness of fit	0.830	1.128	1.098
$\Delta\rho_{\text{max,min}}$ [e Å ⁻³]	2.063, -1.337	2.208, -1.259	2.261, -1.284

$$^a R_1 = \Sigma ||F_o| - |F_c|| / \Sigma |F_o|. \quad ^b R_w = [\Sigma w (F_o^2 - F_c^2)^2 / \Sigma w (F_o^2)^2]^{1/2}$$

Table S3. Crystallographic parameters of β -1-PF₆

	β -1-PF ₆ _100K	β -1-PF ₆ _180K	β -1-PF ₆ _180K_13h
Empirical formula	C ₁₃ H ₃₁ F ₆ N ₄ O ₂ PPt		
Formula weight	615.48		
Crystal system	Orthorhombic	Orthorhombic	Orthorhombic
Space group	<i>Pccn</i>	<i>Pccn</i>	<i>P2₁/c</i>
<i>a</i> [Å]	17.4388(14)	17.6257(10)	17.755(4)
<i>b</i> [Å]	18.6569(16)	18.6823(10)	18.578(4)
<i>c</i> [Å]	13.0238(11)	13.1228(7)	13.178(3)
β [°]	90	90	91.354(3)
<i>V</i> [Å ³]	4237.3(6)	4321.2(4)	4345.6(14)
<i>Z</i>	8	8	8
ρ_{calcd} [g cm ⁻³]	1.930	1.892	1.881
<i>F</i> (000)	2400	2400	2400
Temperature [K]	100	180	180
Reflns collected	23257	23888	21433
Independent reflns	4859	4960	8211
Parameters	249	249	554
<i>R</i> (int)	0.0215	0.0330	0.0413
<i>R</i> ₁ ^{<i>a</i>} , <i>R</i> _w ^{<i>b</i>} (<i>I</i> > 2σ)	0.0166, 0.0378	0.0278, 0.0651	0.0786, 0.1745
<i>R</i> ₁ ^{<i>a</i>} , <i>R</i> _w ^{<i>b</i>} (all data)	0.0191, 0.0387	0.0347, 0.0680	0.1205, 0.1984
Goodness of fit	1.086	1.108	1.119
$\Delta\rho_{\text{max,min}}$ [e Å ⁻³]	0.685, -0.784	1.747, -0.603	4.086, -3.189

$$^a R_1 = \sum ||F_o| - |F_c|| / \sum |F_o|. \quad ^b R_w = [\sum w (F_o^2 - F_c^2)^2 / \sum w (F_o^2)^2]^{1/2}.$$

Table S4. Crystallographic parameters of γ -**1-PF₆** and δ -**1-PF₆**

	γ - 1-PF₆_100K	γ - 1-PF₆_180K	γ - 1-PF₆_180K_1h^b	δ - 1-PF₆_180K
Empirical formula	C ₁₃ H ₃₁ F ₆ N ₄ O ₂ PPt			C ₁₃ H ₃₁ F ₆ N ₄ O ₂ PPt·0.25 (CH ₃ CN)
Formula weight	615.48			625.74
Crystal system	Monoclinic	Monoclinic	Monoclinic	Monoclinic
Space group	<i>P</i> 2 ₁ / <i>c</i>	<i>P</i> 2 ₁ / <i>c</i>	<i>P</i> 2 ₁ / <i>c</i>	<i>P</i> 2 ₁ / <i>c</i>
<i>a</i> [Å]	12.3102(10)	12.4109(7)	12.6135(16)	12.5100(12)
<i>b</i> [Å]	12.4943(10)	12.4489(7)	12.2111(16)	12.4582(12)
<i>c</i> [Å]	29.055(2)	29.1607(17)	28.987(4)	29.139(3)
β [°]	92.0630(10)	91.4980(10)	90.196(2)	91.6770(10)
<i>V</i> [Å ³]	4466.0(6)	4503.9(4)	4464.7(10)	4539.4(8)
<i>Z</i>	8	8	8	2
ρ_{calcd} [g cm ⁻³]	1.831	1.815	1.831	1.831
<i>F</i> (000)	2400	2400	2400	2444
Temperature [K]	100	180	180	180
Reflns collected	24968	25143	25242	20876
Independent reflns	9815	9895	10179	7991
Parameters	497	497	718	524
<i>R</i> (int)	0.0181	0.0239	0.0438	0.0438
<i>R</i> ₁ ^{<i>a</i>} , <i>R</i> _w ^{<i>b</i>} (<i>I</i> > 2σ)	0.0185, 0.0379	0.0242, 0.0525	0.0749, 0.1990	0.0404, 0.0996
<i>R</i> ₁ ^{<i>a</i>} , <i>R</i> _w ^{<i>b</i>} (all data)	0.0208, 0.0384	0.0289, 0.0539	0.1286, 0.2305	0.0422, 0.1005
Goodness of fit	1.130	1.077	1.021	1.136
$\Delta\rho_{\text{max,min}}$ [e Å ⁻³]	1.160, -0.648	1.167, -0.596	3.856, -1.096	2.136, -1.696

^a $R_1 = \sum ||F_o| - |F_c|| / \sum |F_o|$. ^b $R_w = [\sum w (F_o^2 - F_c^2)^2 / \sum w (F_o^2)^2]^{1/2}$. ^bLow quality data.

Table S5. Crystallographic parameters of **1-Tf₂N**

	1-Tf₂N_100K	1-Tf₂N_100K_1h	1-Tf₂N_180K
Empirical formula	C ₁₅ H ₃₁ F ₆ N ₅ O ₆ PtS ₂		
Formula weight	750.66		
Crystal system	Monoclinic	Monoclinic	Monoclinic
Space group	<i>P2₁/c</i>	<i>P2₁/c</i>	<i>P2₁/c</i>
<i>a</i> [Å]	12.2283(12)	12.1488(14)	12.1398(16)
<i>b</i> [Å]	13.0239(13)	13.1394(15)	13.1382(18)
<i>c</i> [Å]	16.6075(16)	16.809(2)	16.978(2)
β [°]	103.4780(10)	103.397(2)	102.167(2)
<i>V</i> [Å ³]	2572.1(4)	2610.2(5)	2647.1(6)
<i>Z</i>	4	4	4
ρ_{calcd} [g cm ⁻³]	1.939	1.910	1.884
<i>F</i> (000)	1472	1472	1472
Temperature [K]	100	100	180
Reflns collected	14308	14593	14813
Independent reflns	5671	5754	5828
Parameters	321	507	397
<i>R</i> (int)	0.0172	0.0323	0.0229
<i>R</i> ₁ ^{<i>a</i>} , <i>R</i> _w ^{<i>b</i>} (<i>I</i> > 2σ)	0.0160, 0.0404	0.0390, 0.1002	0.0308, 0.0827
<i>R</i> ₁ ^{<i>a</i>} , <i>R</i> _w ^{<i>b</i>} (all data)	0.0172, 0.0410	0.0521, 0.1100	0.0349, 0.0859
Goodness of fit	1.036	1.011	1.060
$\Delta\rho_{\text{max,min}}$ [e Å ⁻³]	1.566, -0.799	2.044, -0.777	1.752, -0.883

$$^a R_1 = \Sigma ||F_o| - |F_c|| / \Sigma |F_o|. \quad ^b R_w = [\Sigma w (F_o^2 - F_c^2)^2 / \Sigma w (F_o^2)^2]^{1/2}$$